JOURNAL OF Materials CHEMISTRY

Synthesis, crystal structure and magnetic properties of the novel stacking variant lamellar lead oxovanadium phosphate hydrate β-$Pb(VOPO_4)_2{\cdot}4H_2O$. Crystal chemical relationships with related intercalated $M(VOPO_4)_2{\cdot}yH_2O$ compounds

E. Le Fur and J. Y. Pivan*

Laboratoire de Physicochimie, Ecole Nationale Supérieure de Chimie de Rennes, Campus de Beaulieu, Avenue du Général Leclerc, Rennes 35700, France.
E-mail: jean-yves.pivan@ensc-rennes.fr

Received 8th February 1999, Accepted 7th June 1999

The new lamellar vanadium(IV) phosphate β-$Pb(VOPO_4)_2{\cdot}4H_2O$ has been isolated and X-ray single crystal diffraction data gave an orthorhombic cell [space group $P2_12_12_1$, $Z=4$; $a=6.377(9)$, $b=6.384(1)$, $c=25.357(11)$ Å]. The structure, solved by using direct methods and refined to the reliability factors $R_1=0.027$ ($wR_2=0.074$), is a stacking variant of the monoclinic derivative $Pb(VOPO_4)_2{\cdot}4H_2O$ described previously. Magnetic measurements in the range 3–300 K give a magnetic moment consistent with V(IV) cations with weak antiferromagnetic interactions below 6 K. Crystal chemical relationships with related $M(VOPO_4)_2{\cdot}yH_2O$ phosphates are also discussed.

Introduction

The growing number of publications on the vanadium oxide phosphate system V–P–O reflects the relevant interest of these compounds owing to their chemical activity and (or) physical properties, *e.g.* catalysis, ion exchange, intercalation chemistry, low dimensional magnetism. The various coordination polyhedra attainable for the vanadium ions, in relation to their different oxidation states, coupled with the acidic properties of the phosphate species $H_xPO_4^{(3-x)-}$ have resulted in a wide structural variability.[1–24] Thus, depending upon the preparative route [high-temperature solid state reactions, soft hydrothermal treatments with (or without) addition of organic templates, redox intercalation reactions], different connectivities between the vanadium and phosphorus polyhedra have been evidenced in often complex polyhedral frameworks. While three dimensional (3D) condensed phases are more easily attainable from high-temperature solid-state reactions,[25–31] the overall topology can be tailored, when using soft hydrothermal conditions, to two dimensional (2D) [*e.g.* lamellar phosphates such as $VOPO_4{\cdot}2H_2O$ and the intercalated derivatives $M_x(VOPO_4)_2{\cdot}yH_2O$ (M alkali, alkaline-earth or transition element)[11–16]], one dimensional (1D) [*e.g.* $[H_3N(CH_2)_2NH_3]V(OH)(HPO_4)_2{\cdot}H_2O$ with V–OH–V chains[32]] and even isolated (0D) species [*e.g.* $VO(HPO_4){\cdot}0.5H_2O$ which exhibits isolated face-shared bioctahedral units[33]]. As a consequence, the chemical activity as well as the physical properties are closely related to the preparative strategy. In the course of our investigations on the Pb–V–P–O system, we have synthesized two new lead vanadium phosphates: $Pb(OH)V(HPO_4)_2$ with vanadium(III) ions[34] and the vanadium(IV) lamellar derivative β-$Pb(VOPO_4)_2{\cdot}4H_2O$, in addition to the lamellar $Pb(VOPO_4)_2{\cdot}4H_2O$ and $Pb(VOPO_4)_2{\cdot}3H_2O$, previously reported by Lii *et al.*[9] The present paper reports the single crystal structure and magnetic properties of the new 2D oxovanadium phosphate hydrate β-$Pb(VOPO_4)_2{\cdot}4H_2O$.

Experimental

Synthesis

A mixture of V_2O_5 (0.1535 g, 0.84 mmol), vanadium metal (−325 mesh), $PbCO_3$, 85% aqueous H_3PO_4, tetraethylammonium chloride and water in the mole ratio $1.12:1:14.7:6.03:\approx 200$ was introduced into a Teflon acid digestion bomb (23 ml) and heated at 235 °C for 72 h under autogenous pressure. The final product was filtered off and recovered as a greenish-blue powder along with small platelet single crystals suitable for accurate structural analysis. The X-ray powder pattern, performed on the bulk material, was obviously different from that of the monoclinic $Pb(VOPO_4)_2{\cdot}4H_2O$ reported by Lii and coworkers.[9] All the peaks observed on the powder diffractogram could be accounted for on the basis of the pseudo-tetragonal unit cell found from single-crystal studies.

Susceptibility measurements

Zero-field cooled susceptibility measurements were conducted on 80 mg of manually selected single crystals of β-$Pb(VOPO_4)_2{\cdot}4H_2O$. The magnetic susceptibility data were recorded over the temperature range 2–300 K in a magnetic field of 1 kG using a SQUID magnetometer. The susceptibility data show a broad maximum at $T\approx 6.4$ K which is indicative of magnetic interactions at low temperature. The negative deviation of the corresponding χT curve with temperature below 50 K shows that the prevailing interactions are antiferromagnetic. The high temperature part of the reciprocal susceptibility *vs.* temperature curve is well fitted by a Curie–Weiss law $\chi = C/(T-\theta)$ with an experimental magnetic moment in very good agreement with that expected for V^{IV} ions ($\mu_{exp}=1.74\ \mu_B$, $\mu_{theor}=1.73\ \mu_B$). The data have been fitted using the equation according to Rushbrooke and Wood[35] for an $S=½$ square planar Heisenberg lattice:

$$\chi\cdot\left[1-\frac{2}{x}+\frac{2}{x^2}-\frac{4}{(3x^3)}+\frac{1}{(4x^4)}+\frac{0.4833}{x^5}+\frac{0.003797}{x^6}\right]=\frac{Ng^2\beta^2}{4k_BT};\quad (x=k_BT/J) \tag{1}$$

The best fit, obtained for $J=-1.75\ cm^{-1}$, compares well with previous J values for similar antiferromagnetic layered oxovanadium(IV) phosphates $M(VOPO_4)_2{\cdot}4H_2O$[20,36,37] [$J=-1.74\ cm^{-1}$ for $Sr(VOPO_4)_2{\cdot}4H_2O$,[20] $-1.95\ cm^{-1}$ for α-$Pb(VOPO_4)_2{\cdot}4H_2O$,[36] $-2.01\ cm^{-1}$ for $Ca(VOPO_4)_2{\cdot}4H_2O$,[36] $-1.45\ cm^{-1}$ for $Ba(VOPO_4)_2{\cdot}4H_2O$,[36] $-1.93\ cm^{-1}$ for (Zn,

Mg)$(VOPO_4)_2{\cdot}4H_2O$[37]]. The corresponding χ^{-1} *vs.* T and χT *vs.* T curves are shown in Fig. 1.

Thermal analysis

Thermogravimetry (TG) was performed on powder samples of β-$Pb(VOPO_4)_2{\cdot}4H_2O$ in flowing N_2 up to 1153 K with a heating rate of 1 K min^{-1}. A continuous weight loss of 10% was observed between 450 and 750 K due to loss of water. The decomposition product was identified by X-ray powder analysis as the anhydrous $Pb(VOPO_4)_2$.[38] The initial stoichiometry derived from thermogravimetry is $Pb(VOPO_4)_2{\cdot}3.3H_2O$. Slight variations in water content are commonly found in these types of compounds,[13] and in the following the formula is represented as $Pb(VOPO_4)_2{\cdot}4H_2O$ according to the structural results.

Single-crystal X-ray diffraction and structure determination

The crystal structure of β-$Pb(VOPO_4)_2{\cdot}4H_2O$ was determined from single-crystal X-ray diffraction data. A well shaped crystal was mounted on a glass fiber for intensity data collection on an Enraf-Nonius Cad4 diffractometer. The unit cell was obtained from the least-squares refinement of 25 accurately measured reflections collected within the range 5–12°. Intensity data were recorded at room temperature, in the $\omega-2\theta$ scanning mode with standard reflections monitored for intensity and orientation changes during data collection. Data reduction was performed with the MolEN program,[39] the data were routinely corrected for Lorentz-polarization effects and corrected for absorption by using the ψ-scan method.[40] The crystallographic data, conditions for intensity data collection, structure solution and refinement are given in Table 1. The orthorhombic symmetry was confirmed by comparison of the intensity of equivalent reflections. The systematic absent reflections for $h00$, $0k0$, $00l$ with $h=2n+1$, $k=2n+1$, $l=2n+1$, respectively, indicated $P2_12_12_1$ as the unique space group. SHELXS-86[41] was used to solve the structure (direct methods) and refinement was performed against F^2 using the program SHELXL-97.[42]

After the positional coordinates, isotropic then anisotropic thermal parameters of the non-hydrogen atoms were refined, electron peaks near non-bonded oxygen atoms were unambiguously attributed to hydrogen atoms. The refinement converged at $R_1=0.027$ and $wR_2=0.074$. At the end of refinement, the maximum electron residuals were located near the lead atom (-2.47 e Å^{-3} at $d\approx1.2$ Å; $+3.65$ e Å^{-3} at $d\approx0.9$ Å). Final atomic coordinates are given in Table 2, and selected bond distances and angles and bond valence sums[43] are listed in Table 3. Full crystallographic details, excluding structure factors, have been deposited at the Cambridge Crystallographic Data Centre (CCDC). See

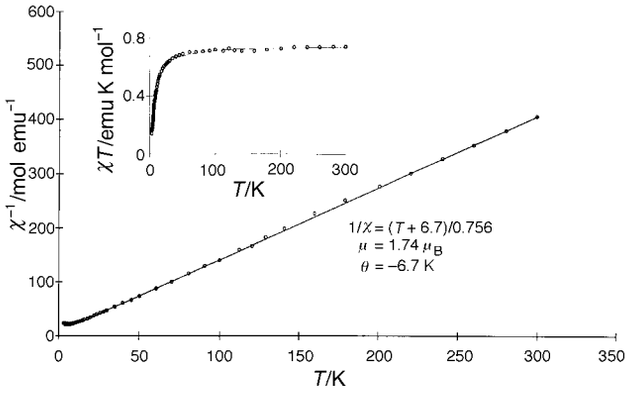

Fig. 1 The χ^{-1} *vs.* T curve (inset: χT *vs.* T) for β-$Pb(VOPO_4)_2{\cdot}4H_2O$. Open circles are experimental points, the full line represents the fit according to the 2D Heisenberg model.

Table 1 Crystal data for β-$Pb(VOPO_4)_2{\cdot}4H_2O$

(i) Crystal data

Chemical formula	$PbV_2P_2O_{14}H_8$
Color, habit	Greenish-blue, plate-like
Crystal system	Orthorhombic
Space group	$P2_12_12_1$ (no. 19)
Unit cell dimensions	
a/Å	6.377(9)
b/Å	6.384(1)
c/Å	25.357(11)
V/Å^3	1032.4(15)
Z	4
M	603.08
D_c/g cm^{-3}	3.88

(ii) Data collection, structure solution and refinement

μ(Mo-Kα)/cm^{-1}	184.3
Radiation (λ/Å)	Mo-Kα (0.71073)
2θ/°	$\leqslant 60$
Data collected	h: 0–8; k: −8 to 8; l: 0–35
Total data	2966
Observed data	2220 [$F^2>2.0\sigma(F^2)$]
R_{int}	0.0232
Residuals[a]	$R_1=0.027$, $wR_2=0.074$
GOF	1.025

[a] $R_1=\Sigma||F_o|-|F_c||/\Sigma|F_o|$; $wR_2=[w(F_o^2-F_c^2)/w(F_o^2)]^{1/2}$ with $w=1/[\sigma^2(F_o^2)+(0.063P)^2]$; $P=(\max(F_o^2,0)+2F_c^2)/3$.

Table 2 Atomic coordinates and equivalent isotropic displacement coefficients U_{eq}[a] with estimated standard deviations in parentheses

Atom	x	y	z	U_{eq}/10^2 Å^2
Pb	0.87692(5)	0.11769(4)	0.12427(1)	1.90(1)
V1	0.24949(22)	0.34079(17)	0.22762(5)	0.67(2)
V2	0.15197(19	0.00274(18)	0.97779(5)	0.71(2)
P1	0.65553(28)	0.99992(26)	0.99851(7)	0.66(3)
P2	0.75055(31)	0.34005(26)	0.24943(7)	0.69(4)
O1	0.9396(9)	0.3306(9)	0.2114(2)	1.06(11)
O2	0.2417(10)	0.0346(8)	0.2153(2)	1.02(10)
O3	0.7566(10)	0.8550(9)	0.2095(2)	1.57(11)
O4	0.5570(9)	0.3364(9)	0.2130(2)	1.15(11)
O5	0.2516(10)	0.6510(8)	0.2123(2)	1.18(10)
O6	0.1359(11)	0.0100(9)	0.0410(2)	1.81(11)
O7	0.8443(9)	0.9988(9)	0.9598(2)	1.15(11)
O8	0.4589(9)	0.0069(9)	0.9641(2)	1.22(11)
O9	0.6652(9)	0.1888(8)	0.0367(2)	1.11(11)
O10	0.6574(10)	0.8163(8)	0.0345(2)	1.10(11)
Ow1	0.0159(10)	0.7399(8)	0.1274(3)	1.23(18)
Ow2	0.4906(10)	0.9574(9)	0.1246(3)	2.06(19)
Ow3	0.2522(10)	0.3008(8)	0.1332(2)	1.25(16)
Ow4	0.6786(9)	0.4960(10)	0.1152(2)	1.57(18)
H1	0.499	0.039	0.126	5[b]
H2	0.403	0.888	0.123	5[b]
H3	0.087	0.796	0.113	5[b]
H4	0.644	0.547	0.120	5[b]
H5	0.115	0.702	0.147	5[b]
H6	0.202	0.339	0.129	5[b]
H7	0.343	0.202	0.129	5[b]
H8	0.574	0.412	0.124	5[b]

[a] U_{eq} is defined as one-third of the trace of the orthogonalized U_{ij} tensor. [b] Value fixed.

Information for Authors, 1999, Issue 1. Any request to the CCDC for this material should quote the full literature citation and the reference number 1145/165. See http://www.rsc.org/suppdata/jm/1999/2589/ for crystallographic files in .cif format.

Bond valence sums are in agreement with the formal oxidation states for the vanadium and phosphorus centres. As previously observed by Lii and coworkers[9] for α-$Pb(VOPO_4)_2{\cdot}4H_2O$, the obtained value ($\Sigma s=1.7$) for the Pb^{2+} cation is somewhat lower than the expected value of 2. This result can be ascribed largely to a poorly refined location of the Pb^{2+} cation owing to the stereochemical activity of the

Table 3 Selected bond lengths (Å) and bond angles (°) with estimated standard deviation in parentheses and bond valence sums (Σs) for β-$Pb(VOPO_4)_2{\cdot}4H_2O$

Pb	Distance	Angles						
Ow1	2.571(5)							
O1	2.625(6)	114.0(2)						
O9	2.637(6)	111.4(2)	134.2(2)					
Ow2	2.668(8)	87.6(2)	109.7(2)	66.2(2)				
Ow3	2.673(7)	95.7(2)	64.2(2)	117.0(2)	173.9(2)			
Ow4	2.736(6)	172.0(2)	71.6(2)	62.6(2)	84.9(2)	92.0(2)		
O6	2.767(7)	65.5(2)	132.9(2)	72.9(2)	117.2(2)	68.9(2)	115.5(2)	
O3	2.842(7)	61.1(2)	72.9(2)	127.2(2)	61.5(2)	115.8(2)	117.4(2)	126.5(2)
	Pb	Ow1	O1	O9	Ow2	Ow3	Ow4	O6
Σs(Pb–O)	1.72							
V1	Distance	Angles						
O3	1.597(6)							
O2	1.980(6)	102.3(3)						
O4	1.996(7)	102.1(3)	88.9(3)					
O1	2.020(7)	100.4(3)	84.9(3)	157.4(2)				
O5	2.018(6)	97.9(3)	159.8(2)	88.4(3)	89.9(3)			
Ow3	2.407(6)	177.0(3)	74.8(2)	78.4(2)	78.5(2)	85.0(2)		
	V1	O3	O2	O4	O1	O5		
Σs(V–O)	4.06							
V2	Distance	Angles						
O6	1.608(6)							
O8	1.988(7)	103.7(3)						
O10	1.998(5)	100.7(3)	88.2(3)					
O9	2.005(5)	99.1(3)	85.0(2)	160.1(2)				
O7	2.014(6)	99.5(3)	156.9(2)	88.2(3)	90.7(2)			
Ow4	2.363(6)	178.1(3)	75.8(2)	81.2(2)	79.1(2)	81.1(2)		
	V2	O6	O8	O10	O9	O7		
Σs(V–O)	4.04							
P1	Distance	Angles						
O8	1.529(6)							
O10	1.537(6)	111.7(4)						
O9	1.549(6)	111.6(4)	104.7(3)					
O7	1.553(6)	106.0(3)	111.5(3)	111.6(3)				
	P1	O8	O10	O9				
Σs(P–O)	4.90							
P2	Distance	Angles						
O2	1.531(5)							
O4	1.542(6)	112.8(3)						
O1	1.545(6)	111.8(3)	104.5(3)					
O5	1.550(5)	105.4(3)	110.9(3)	111.6(3)				
	P2	O2	O4	O1				
Σs(P–O)	4.90							

$6s^2$ lone pair[44] (reflected in the high residuals found near the lead position). Indeed, on the basis of the external electronic structure for Pb^{2+} ($6s^26p^0$), the Pb^{2+} cation is better described as a Pb^{4+} core cation with a stereoactive $6s^2$ lone pair. As a consequence, the Pb^{4+} core cation can be significantly displaced from the position obtained from X-ray structural analysis. When accounting for the resulting modifications in the Pb–O bond distances, a correct bond sum valence of 2 can be readily obtained.

The vanadium atoms are coordinated to five oxygen atoms to form familiar planar pyramids characteristic of the vanadyl ion with a very short V=O bond distance ($\approx$1.6 Å). The four basal oxygen, at distances of *ca.* 2.0 Å, are shared with four PO_4^{3-} tetrahedra to generate a 4-connected net. The near neighbouring of the vanadium ions is completed by weakly bonded interlayer water molecules ($d \approx 2.4$ Å) *trans* to the short V=O bond. The P–O bond distances range from 1.529(6) to 1.553(6) Å with an average value of 1.54 Å in very good agreement with P–O distances reported for orthophosphate compounds. The lead cations, located between the layers, are coordinated to eight oxygen atoms with Pb–O distances ranging from 2.571(5) to 2.842(7) Å.

Crystal chemical study and discussion

The structure of the title compound, shown in Fig. 2, is closely related to that of the highly symmetric parent structure of $VOPO_4{\cdot}2H_2O$ which has a tetragonal unit cell with parameters $a = 6.21$ Å and $c = 7.41$ Å. The structure of $VOPO_4{\cdot}2H_2O$[45]

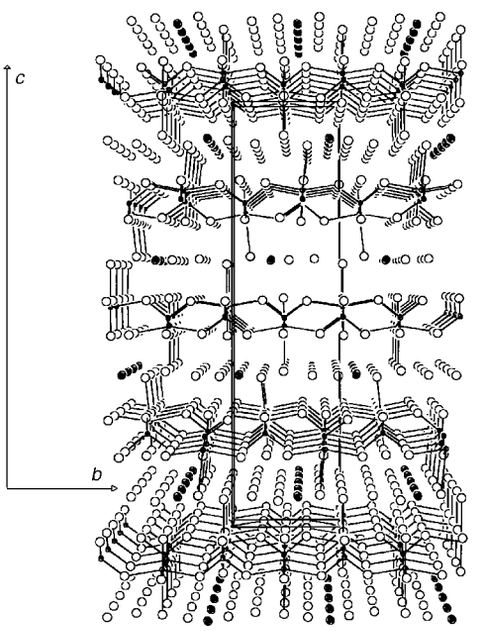

Fig. 2 The structure of β-$Pb(VOPO_4)_2{\cdot}4H_2O$ viewed along the [100] direction. Thermal ellipsoids with shaded segments are Pb cations. The V–O and P–O bonds are represented by full lines.

is a 4-connected net of alternated corner-shared vanadium $O{=}VO_{4/2}(OH_2)$ and phosphorus $PO_{4/2}$ polyhedra with additional water molecules between the layers. The lamellar compounds $M(VOPO_4)\cdot yH_2O$ (MVPOs) consist of successive negatively charged layers $[VOPO_4]^{u-}$ counterbalanced by positively charged layers $[M(H_2O)_y]^{u+}$ which are distributed as a quasi-perfect square planar sublattice with edges denoted $\boldsymbol{a}$ and $\boldsymbol{b}$ (Fig. 3). The 4-connected layers $[VOPO_4]^{u-}$ are essentially unchanged upon intercalation of cations; nevertheless their stacking is strongly interdependent with that of the positive layers $[M(H_2O)_y]^{u+}$. The stacking sequence vector $\boldsymbol{S}$ is approximately perpendicular to the layers with values $\boldsymbol{S}\approx n\times\boldsymbol{d}$ where the interlayer separation $\boldsymbol{d}$ ranges from 7.41 Å in $VOPO_4\cdot 2H_2O$ to 6.30 Å in the triclinic CaVPO.[9] Different polymorphic forms of the MVPOs are known, with cell volumes $V\approx 255$ Å^3 ($n=1$) as found for the triclinic variants CaVPO and (Zn, Mg)VPO;[46] $V\approx 520$ Å^3 ($n=2$) as reported for the tetragonal CoVPO,[9] monoclinic BaVPO[21,47] or triclinic NaVPO.[6] The β-PbVPO structure with a cell volume $V=1033$ Å^3 is the first example with $n=4$.

The structural relationships between the different polymorphs are discussed according to the relative displacements of the positive layers $[M(H_2O)_y]^{u+}$. Though the stacking vector $\boldsymbol{S}$ is perpendicular to the layers for CoVPO, BaVPO and β-PbVPO, the relative displacements of the layers are somewhat different for these three structures which results in different unit cell dimensions and symmetries.

The structures of KVPO, NaVPO, (Zn, Mg)VPO, CaVPO and α-PbVPO, for which the angle between the stacking vector $\boldsymbol{S}$ and the $[M(H_2O)_y]^{u+}$ plane slightly deviates from 90°, differ from each other for the same reasons. For the K^+, $(Zn, Mg)^{2+}$ and Ca^{2+} derivatives, the successive $[M(H_2O)_y]^{u+}$ layers are slightly shifted from each other by a constant distance. When a projection is made along the stacking direction $\boldsymbol{S}$, the different layers can be superimposed and consequently, the magnitude of the stacking vector ($\boldsymbol{S}\approx 6.6$ Å) is roughly the same as the interlayer separation ($\boldsymbol{d}\approx 6.5$ Å), with cell volumes $V\approx 255$ Å^3 [$V=251.9$, 263.7 and 253.9 Å^3 for K^+, $(Zn, Mg)^{2+}$ and Ca^{2+} structures, respectively].

For α-PbVPO, the successive layers are displaced from each other as already pointed out by Lii *et al.*,[9] in an alternated way, by $\boldsymbol{T_1}\approx(\boldsymbol{a}+\boldsymbol{b})/4$ and $\boldsymbol{T_2}\approx-(\boldsymbol{a}+\boldsymbol{b})/4$. The same behavior is seen for the structure of NaVPO but two successive layers are displaced in an alternated way by $\boldsymbol{T_1}\approx\boldsymbol{a}/6$ and $\boldsymbol{T_2}\approx-\boldsymbol{a}/6$. For these latter two structures, $\boldsymbol{T_1}$ is not exactly counterbalanced by

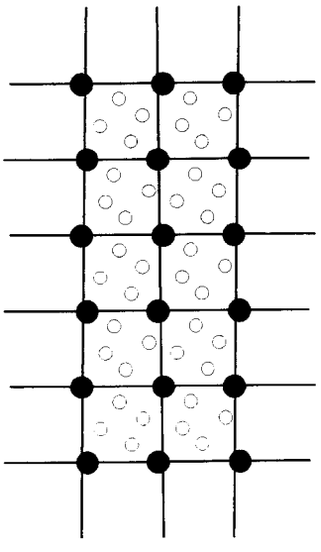

Fig. 3 Partial view along the [001] direction of the $[Ba(H_2O)_4]^{2+}$ layer showing the square planar sublattice of the Ba^{2+} cations in BaVPO. Large black circles are barium cations, small open circles represent the water molecules.

Table 4 Selected crystallographic data for MVPO structures

Compound	Cell parameters	Space group	Cell volume/Å^3	Rotation sequence	V–V (intralayer)/Å	V–V (interlayer)/Å	$\boldsymbol{S}$ vector/Å	Location of the cation[a]	Ref.
$Na(VOPO_4)_2\cdot 4H_2O$	6.285, 6.284, 13.262 Å, 80.30, 87.43, 89.94°	$P\bar{1}$	515.7	$+\alpha$	4.61	6.093	13.262	D	6
$K(VOPO_4)_2\cdot 3H_2O$	6.282, 6.285, 6.679 Å, 89.11, 72.84, 89.98°	$P\bar{1}$	251.9	$+\alpha$	4.61	6.054	6.679	S	6
$Ca(VOPO_4)_2\cdot 4H_2O$	6.348, 6.350, 6.597 Å, 106.8, 94.09, 90.02°	$P1$	253.9	$+\alpha$	4.61	5.961	6.597	S	9
$Sr(VOPO_4)_2\cdot 4H_2O$	9.026, 9.010, 12.841 Å, 100.19°	Cc	1027.8[b]	$+\alpha, -\beta$	4.65	5.900	12.841	S	9
$Ba(VOPO_4)_2\cdot 4H_2O$	6.376, 12.754, 9.006 Å, 135.03°	Pc	521.2	$+\alpha, -\alpha$	4.64	5.900	12.754	S	21, 47
α-$Pb(VOPO_4)_2\cdot 4H_2O$	9.030, 9.021, 12.874 Å, 100.16°	Cc	1032.3[b]	$+\alpha, -\beta$	4.65	5.900	12.874	S	9
β-$Pb(VOPO_4)_2\cdot 4H_2O$	6.377, 6.384, 25.357 Å	$P2_12_12_1$	1032.4	$+\alpha, +\alpha, -\alpha, -\alpha$	4.65	5.890	25.357	D, S	This work
$Co(VOPO_4)_2\cdot 4H_2O$[c]	6.264, 6.264, 13.428 Å	$I4/mmm$	526.9	$+\alpha$	4.50	5.959	13.428	S	9
$Cu(VOPO_4)_2\cdot 4H_2O$[b]	6.614, 8.930, 9.071 Å, 103.79°	$P2_1/m$	520.3	$+\alpha$	≈4.6	6.110	6.614	S	32
(Mg, Zn)$(VOPO_4)_2\cdot 4H_2O$	6.251, 6.258, 8.065 Å, 112.85, 112.86, 89.93°	$P1$	263.7	$+\alpha$	4.48	5.993	8.070	S	46

[a]For the location of the intercalated cation, the symbol S indicates one location inside the windows and D more than one location inside the windows. [b]The cell volumes of the Sr^{2+}, Cu^{2+} and Pb^{2+} compounds are twice the ideal value owing to supplementary superstructure. [c]Disordered tetragonal structure; the true structure is more likely triclinic with parameters very close to those for $(Mg,Zn)(VOPO_4)_2\cdot 4H_2O$.

$\boldsymbol{T_2}$ so that $\boldsymbol{S}$ is not perpendicular to the $[M(H_2O)_4]^{u+}$ layers (angles of 100.16 and 80.30°, respectively) and $\boldsymbol{S}$ is twice that of the Ca^{2+} derivative [$\boldsymbol{S}$ = 12.874 Å (Pb^{2+}) and 13.262 Å (Na^{+})]. The expected volume $V_{theor} \approx 2 \times 255$ Å^3 agrees fairly well with $V_{exp} = 515.7$ Å^3 (Na^{+}) and the normalized $V_{exp} = 526$ Å^3 (Pb^{2+} compound when taking into account the additional supercell described by Lii *et al.*[9]). For the BaVPO and CoVPO structures, the displacements of the layers are $\boldsymbol{T_1} \approx (\boldsymbol{a}+\boldsymbol{b})/2$, $\boldsymbol{T_2} \approx -(\boldsymbol{a}+\boldsymbol{b})/2$, with cell volumes of 517.6 and 526.9 Å^3, respectively. $\boldsymbol{T_1}$ is exactly counterbalanced by $\boldsymbol{T_2}$ so $\boldsymbol{S}$ is perpendicular to the $[M(H_2O)_4]^{2+}$ layers and $\boldsymbol{S}$ is doubled [$\boldsymbol{S}$ = 12.754 Å (Ba^{2+}) and 13.428 (Co^{2+})].

For the β-PbVPO structure, four translation vectors $\boldsymbol{T_1}$, $\boldsymbol{T_2}$, $\boldsymbol{T_3}$ and $\boldsymbol{T_4}$ are present which lead to an $\boldsymbol{S}$ vector four times that of CaVPO. The expected volume $V_{theor} \approx 4 \times 255$ Å^3 is very close to the experimental volume, $V = 1033$ Å^3. The respective magnitude and direction of the $\boldsymbol{T_i}$ vectors are $\boldsymbol{T_1} \approx \boldsymbol{a}/4 + \boldsymbol{b}/2$, $\boldsymbol{T_2} \approx \boldsymbol{a}/2 + \boldsymbol{b}/4$, $\mathbf{T}_3 \approx -\boldsymbol{a}/4 + \boldsymbol{b}/2$, $\boldsymbol{T_4} \approx \boldsymbol{a}/2 - \boldsymbol{b}/4$ with $\boldsymbol{T_2} > \boldsymbol{T_1}$ and $\boldsymbol{T_4} > \boldsymbol{T_3}$. The overall displacement $\boldsymbol{T_1} + \boldsymbol{T_2} + \boldsymbol{T_3} + \boldsymbol{T_4}$ is null so that $\boldsymbol{S}$ is perpendicular to the $[Pb(H_2O)_4]^{2+}$ layers.

When comparing the different displacements for the β-PbVPO and α-PbVPO structures, they can be thought of as polytypes. These subtle differences between the relative displacements of the $[M(H_2O)_4]^{u+}$ layers coupled to those of the adjacent $[VOPO_4]^{u-}$ layers result in slight topological modifications. Fig. 4 shows the overall framework of various representatives of MVPO structures in projection parallel to the $\boldsymbol{a}$ (or) $\boldsymbol{b}$ direction relative to the cation square planar sublattice. As can be seen in Table 4, all the structures are characterized by short intralayer V–V bond distances of *ca.* 4.6 Å which participate to a large extent in low dimensional magnetism *via* phosphate bridges. Another set of V–V distances remains essentially constant for all the structures corresponding to the shortest interlayer V–V linkages with values of *ca.* 6 Å. When considering these short V–V distances,

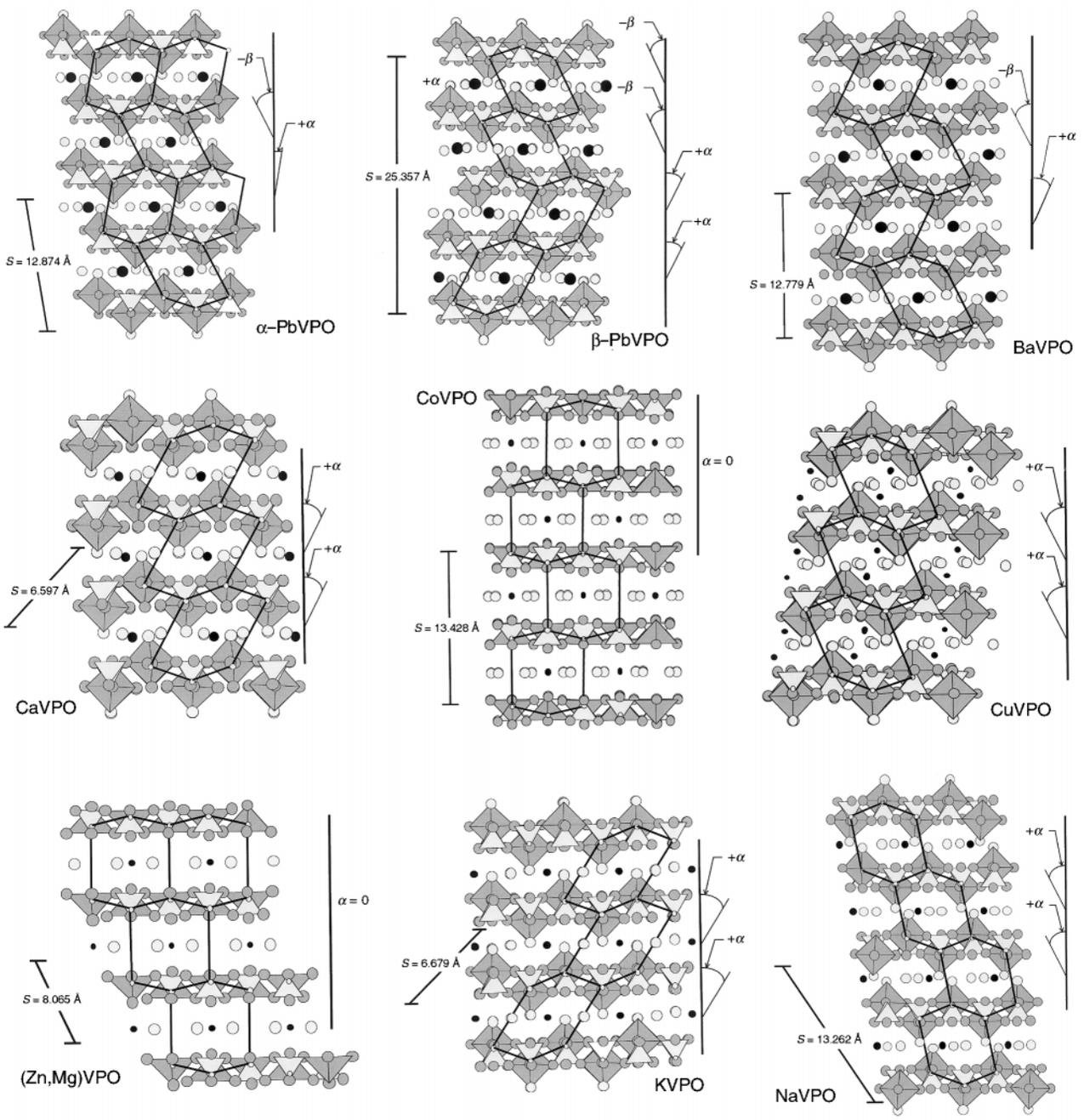

Fig. 4 The structures of MVPOs viewed along $\boldsymbol{a}$ (or $\boldsymbol{b}$) relative to the cation square planar sublattice. The vanadium and phosphorus polyhedra are emphasized. Open circles are water molecules, black circles are the intercalated cations.

the structures can be described by considering more or less distorted windows of hexagonal cross-section (four edges with $d_{V-V} \approx 4.6$ Å and two opposite edges with $d_{V-V} \approx 6$ Å). These windows, elongated parallel to the interlayer V–V distances, are displayed in different ways in the structures. In most cases, the intercalated cations are located approximately at the center of the windows and the windows are rotated with respect to the vector normal to the layers.

Different cases may occur: (i) all the windows are rotated by the same quantity (say $+\alpha$) as found for the structures of CaVPO, (Zn, Mg)VPO, CoVPO, CuVPO, KVPO and NaVPO; (ii) the windows are rotated clockwise ($+\alpha$) and anticlockwise ($-\beta$) as found for the structures of BaVPO, α- and β-PbVPO. If the clockwise ($+\alpha$) rotation is exactly counterbalanced by the anticlockwise ($-\beta$) rotation (*i.e.* $|\alpha| = |\beta|$), the stacking vector $\boldsymbol{S}$ is perpendicular to the layers (β-PbVPO, BaVPO structures), if not, the stacking vector is not perpendicular to the layers (α-PbVPO structure); (iii) the clockwise ($+\alpha$) and the anticlockwise ($-\beta$) sequence of rotations is different as found in the structures of α-PbVPO and β-PbVPO. The sequences are $+\alpha-\beta$ [denoted $(+-)$] for α-PbVPO and $+\alpha+\alpha-\beta-\beta$ [denoted $(++--)$] for β-PbVPO, respectively. It is of note that the sequence $(++-)$ leading to an $\boldsymbol{S}$ vector three times that of Ca^{2+}, has not yet been reported; (iv) the location of the intercalated cations is unchanged inside the window. This is the case for CaVPO, (Zn, Mg)VPO, CoVPO, KVPO and CuVPO; (v) the location of the intercalated cations is changed inside the window as found in NaVPO.

When considering the different combinations (i)–(v), a vast number of polymorphic structures, many, as yet, not reported, is attainable. Application of these criteria to the CoVPO structure shows that it corresponds to cases (i) and (iv) (the windows are rotated by the same quantity and the Co^{2+} cations are located at the same location inside the windows). Such a situation points to a triclinic unit cell with parameters $a \approx b \approx 6.4$ Å, $c \approx 6.6$ Å ($V \approx 260$ Å^3). The disordered tetragonal description of the structure by Lii and coworkers[9] is very likely erroneous. In addition, the fact that the water molecules are eliminated in two well separated steps (thermogravimetry) suggests that the true structure is triclinic as found for (Zn, Mg)VPO.

Conclusion

The crystal structure of the new stacking variant β-Pb($VOPO_4$)$_2$·$4H_2O$ has been solved by X-ray single crystal diffraction data. The susceptibility data shows Curie–Weiss behaviour with the experimental magnetic moment consistent with V^{IV} cations. Weak antiferromagnetic interactions have been evidenced at <6 K. The structural results have been used to develop a crystal chemical study, based upon the relative orientation of pseudo-hexagonal windows, to describe related intercalated M($VOPO_4$)$_2$·yH_2O structures.

Acknowledgements

The authors are indebted to Dr O. Peña for the susceptibility data measurements and Dr L. Ouahab for the single crystal X-ray diffraction data collection.

References

1 G. Centi, F. Trifiro, J. R. Ebner and V. M. Franchetti, *Chem. Rev.*, 1988, **88**, 55.
2 C. C. Torardi, W. M. Reiff and L. Takacs, *J. Solid State Chem.*, 1989, **82**, 203.
3 G. Huan, J. W. Johnson, A. J. Jacobson, E. W. Corcoran, Jr. and D. P. Goshorn, *J. Solid State Chem.*, 1991, **93**, 514, and references therein.
4 K. H. Lii and H. J. Tsai, *J. Solid State Chem.*, 1991, **90**, 291.
5 K. H. Lii, C. H. Lii, C. Y. Cheng and S. L. Wang, *J. Solid State Chem.*, 1991, **95**, 352.
6 S. L. Wang, H. Y. Kang, C. Y. Cheng and K. H. Lii, *Inorg. Chem.*, 1991, **30**, 3496.
7 K. H. Lii and H. J. Tsai, *Inorg. Chem.*, 1991, **30**, 446.
8 K. H. Lii, *J. Chin. Chem. Soc.*, 1992, **39**, 569.
9 H. Y. Kang, W. C. Lee, S. L. Wang and K. H. Lii, *Inorg. Chem.*, 1992, **31**, 4743.
10 K. H. Lii and I. F. Mao, *J. Solid State Chem.*, 1992, **96**, 436.
11 K. H. Lii, S. L. Wu and H. M. Gau, *Inorg. Chem.*, 1993, **32**, 4153.
12 R. C. Haushalter, V. Soghomonian, Q. Chen and J. Zubieta, *J. Solid State Chem.*, 1993, **105**, 512.
13 J. T. Vaughey, W. T. A. Harrison, A. J. Jacobson, D. P. Goshorn and J. W. J. Johnson, *Inorg. Chem.*, 1994, **33**, 2481.
14 W. T. A. Harrison, S. C. Lim, J. T. Vaughey, A. J. Jacobson, D. P. Goshorn and J. W. J. Johnson, *J. Solid State Chem.*, 1994, **113**, 444.
15 Y. Zhang, A. Clearfield and R. C. Haushalter, *J. Solid State Chem.*, 1995, **117**, 157.
16 M. Schindler, W. Joswig and W. H. Baur, *Eur. J. Solid State Inorg. Chem.*, 1995, **32**, 109.
17 W. T. A. Harrison, J. T. Vaughey, A. J. Jacobson, D. P. Goshorn and J. W. J. Johnson, *J. Solid State Chem.*, 1995, **116**, 77.
18 W. T. A. Harrison, S. C. Lim, L. L. Dussack, A. J. Jacobson, D. P. Goshorn and J. W. J. Johnson, *J. Solid State Chem.*, 1995, **118**, 241.
19 A. El Badraoui, J. Y. Pivan, M. Maunaye, M. Louër and D. Louër, *J. Alloys Compd.*, 1996, **245**, 47.
20 D. Papoutsakis, J. E. Jackson and D. G. Nocera, *Inorg. Chem.*, 1996, **35**, 800.
21 M. Roca, M. D. Marcos, P. Amorós, J. Alamo, A. Beltrán-Porter and D. Beltrán-Porter, *Inorg. Chem.*, 1997, **36**, 3414.
22 Z. Bircsak and W. T. A. Harrison, *Acta Crystallogr., Sect. C*, 1998, **54**, 1195.
23 Z. Bircsak and W. T. A. Harrison, *Acta Crystallogr., Sect. C*, 1998, **54**, 1197.
24 Z. Bircsak and W. T. A. Harrison, *Inorg. Chem.*, 1998, **37**, 320.
25 S. Boudin, A. Grandin, A. Leclaire, M. M. Borel and B. Raveau, *J. Mater. Chem.*, 1994, **4**, 1889.
26 S. Boudin, A. Grandin, A. Leclaire, M. M. Borel and B. Raveau, *Acta Crystallogr., Sect. C*, 1994, **50**, 840.
27 S. Boudin, A. Grandin, Ph. Labbé, D. Grebille, N. Nguyen, A. Ducouret and B. Raveau, *J. Solid State Chem.*, 1996, **121**, 291.
28 M. Borel, A. Leclaire, J. Chardon, J. Provost, H. Rebbah and B. Raveau, *J. Solid State Chem.*, 1997, **132**, 41.
29 S. Boudin, A. Grandin, A. Leclaire, M. M. Borel and B. Raveau, *Acta Crystallogr., Sect. C*, 1995, **50**, 796.
30 S. Boudin, A. Grandin, Ph. Labbé, J. Provost and B. Raveau, *J. Solid State Chem.*, 1996, **127**, 330.
31 M. M. Borel, A. Leclaire, J. Chardon and B. Raveau, *J. Mater. Chem.*, 1998, **8**, 693.
32 Y. Zhang, C. J. Warren, A. Clearfield and R. C. Haushalter, *Polyhedron*, 1998, **17**, 2575.
33 M. E. Leonowicz, J. W. Johnson, J. F. Brody, H. F. Shannon, Jr. and J. M. Newsam, *J. Solid State Chem.*, 1985, **56**, 370.
34 E. Le Fur and J. Y. Pivan, unpublished work.
35 G. S. Rusbrooke and P. J. Wood, *Mol. Phys.*, 1958, **1**, 257.
36 M. Roca, P. Amoros, J. Cano, M. D. Marcos, P. Amorós, J. Alamo, A. Beltrán-Porter and D. Beltrán-Porter, *Inorg. Chem.*, 1998, **37**, 3167.
37 E. Le Fur, O. Peña and J. Y. Pivan, *J. Mater. Chem.*, 1999, **9**, 1029.
38 A. Grandin, J. Chardon, M. M. Borel, A. Leclaire and B. Raveau, *Acta Crystallogr., Sect. C*, 1992, **48**, 1913.
39 MolEN (Molecular Structure Enraf-Nonius), Enraf-Nonius, Delft, The Netherlands, 1990.
40 A. C. T. North, D. C. Philips and F. S. Mathews, *Acta Crystallogr., Sect. A*, 1968, **24**, 351.
41 G. M. Sheldrick, SHELXS-86, Program for crystal structure determination, University of Göttingen, Germany, 1986.
42 G. M. Sheldrick, SHELXL-97, Program for crystal structure determination, University of Göttingen, Germany, 1997.
43 I. D. Brown and D. Altermatt, *Acta Crystallogr., Sect. B*, 1985, **41**, 244.
44 E. Morin, G. Wallez, S. Jeaulmes, J. C. Couturier and M. Quarton, *J. Solid State Chem.*, 1998, **137**, 283.
45 H. R. Tietze, *Aust. J. Chem.*, 1981, **34**, 2035.
46 E. Le Fur and J. Y. Pivan, *Mater. Res. Bull.*, 1999, **34**, 97.
47 E. Le Fur, O Peña and J. Y. Pivan, *J. Alloys Compd.*, 1999, **285**, 89.

Paper 9/01048C